Journal of Molecular Catalysis B: Enzymatic 108 (2014) 21–31

Contents lists available at ScienceDirect

Journal of Molecular Catalysis B: Enzymatic

journal homepage: www.elsevier.com/locate/molcatb

Computational study of the enantioselectivity of the *O*-acetylation of (*R*,*S*)-propranolol catalyzed by *Candida antarctica* lipase B

Andrés M. Escorcia[a], Martha C. Daza[a], Markus Doerr[a,b,*]

[a] Grupo de Bioquímica Teórica, Universidad Industrial de Santander, Cra 27, Calle 9, Bucaramanga, Colombia
[b] Grupo de Investigaciones Ambientales para el Desarrollo Sostenible, Universidad Santo Tomás, Cra 18 No. 9-27, Bucaramanga, Colombia

ARTICLE INFO

Article history:
Received 24 January 2014
Received in revised form 16 May 2014
Accepted 21 June 2014
Available online 3 July 2014

Keywords:
Candida antarctica lipase B
O-acylation
Enantioselectivity
Molecular dynamics
Propranolol

ABSTRACT

Candida antarctica lipase B (CalB) displays moderate enantioselectivity when it catalyzes the acetylation of (*R*,*S*)-propranolol, favoring the faster transformation of the *R*-propranolol. With the aim to better understand the enantioselectivity of this reaction, we have performed a molecular dynamics (MD) study of the enzyme substrate complexes. Reactive enzyme substrate complexes were identified for both enantiomers of propranolol, which differ in their temporal stability and in their ability to reach the corresponding transition states (TS). Reactive complexes of *R*-propranolol present a better ability to be transformed by CalB than those of *S*-propranolol. This allows us to explain the enantioselectivity. Analysis of the enzyme–substrate interactions suggests that the CH-π interactions between the naphthyl rings of propranolol and the residues of the CalB binding pocket may play an important role in stabilizing the transition states involved in the transformation of the *R*-propranolol. The residues Ile189, Ala282 and Leu278 were identified as key residues for the enantioselectivity of CalB.

1. Introduction

Propranolol ((*R*,*S*)-1-iso-propylamino-3-(1-naphthoxy)-2-propanol), a beta-adrenergic blocking agent used for treatment of arterial hypertension and other cardiovascular disorders [1–3], is commercially available as a racemic mixture. However, only the *S*-enantiomer has the desired therapeutic effect, and administration of the racemic propranolol mixture may cause side effects such as bronchoconstriction or diabetes [4–6].

Several strategies to obtain *S*-propranolol in enantiomerically pure form have been proposed, including chemical, enzymatic and chemoenzymatic synthesis routes [7–16]. Recently immobilized *Candida antarctica* lipase B (CalB) was used as a biocatalyst to carried out the acetylation of (*R*,*S*)-propranolol in toluene. The enantioselectivity was moderate ($E = 57$), but higher than or comparable to the enantioselectivity observed in the kinetic resolution of propranolol either via esterification or hydrolysis using other enzymes [13]. Using immobilized CalB allows to reuse the biocatalyst and to simplify its separation from the reaction products. This makes the reaction attractive for industrial applications, but the enantioselectivity has to be improved for this purpose.

Lipases are characterized by a catalytic triad consisting of Serine, Histidine and Aspartate (Ser105, His224 and Asp187 in CalB). The accepted general mechanism of lipase-catalyzed reactions involves two steps. The first step of the reaction is the addition of an acyl-group to the catalytic serine of the enzyme, yielding the acyl-enzyme (acylation step). In the second step, the acyl-group can react with several nucleophiles, such as water, alcohols, amines or peroxides (deacylation step) [17]. Acylation as well as deacylation proceed via an initial noncovalent enzyme–substrate complex (Michaelis complex; MCC) and a tetrahedral intermediate (TI). The latter is stabilized by NH and OH functions in the so-called oxyanion hole of the enzyme, constituted by the residues Thr40 and Gln106 in CalB. According to this mechanism, the deacylation step in the CalB-catalyzed acetylation of (*R*,*S*)-propranolol is expected to be chemo- (*N*- or *O*-acetylation) and stereoselective (acetylation of *R*- or *S*-propranolol) (see Scheme 1).

We previously studied the chemoselectivity of this reaction and found experimentally that the *O*-acylated product is formed exclusively [18]. To rationalize this result we applied an enzyme–substrate docking protocol to model the MCCs of the deacylation reaction, which showed that both *R*- and *S*-propranolol accommodate within the binding pocket of CalB in two binding

* Corresponding author at: Grupo de Bioquímica Teórica, Universidad Industrial de Santander, Cra 27, Calle 9, Bucaramanga, Colombia. Tel.: +57 7 6344000x1420.
E-mail addresses: andrescorcia6@hotmail.com (A.M. Escorcia), marthacde@yahoo.com (M.C. Daza), markusdoerr@gmx.de, mhodoerr@uis.edu.co (M. Doerr).

http://dx.doi.org/10.1016/j.molcatb.2014.06.010
1381-1177/

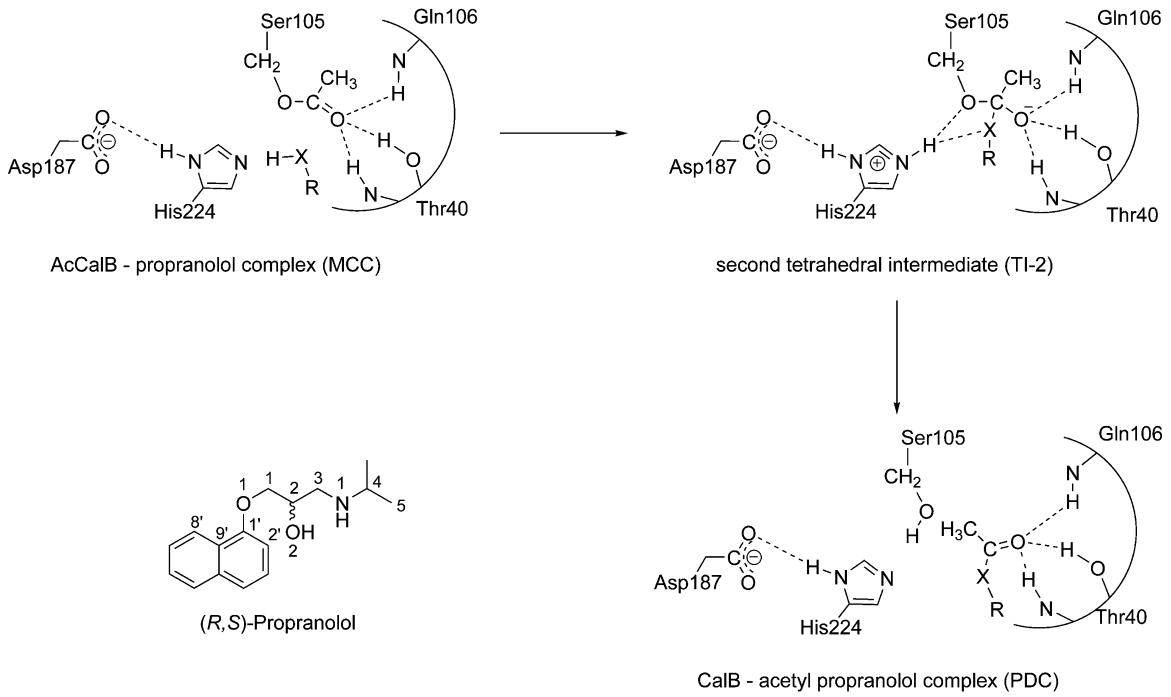

Scheme 1. Deacylation step in the CalB-catalyzed acetylation of (*R,S*)-propranolol (X = N or O, according to the nucleophile groups of propranolol). This reaction step occurs sequentially via an initial noncovalent acetyl-CalB (AcCalB) substrate complex (Michaelis complex; MCC) and the second tetrahedral intermediate (TI-2), to give a noncovalent CalB-product complex (PDC). The structure of propranolol with the corresponding atom numbering is shown down at the left.

modes (namely, binding modes I and II). Viewed with the catalytic triad Asp-His-Ser oriented from left to right, the binding pocket of CalB is constituted by a large hydrophobic pocket above the catalytic triad and a medium size pocket below it. In binding mode I the naphthoxy side chain of propranolol is located in the large hydrophobic pocket. The isopropylamine side chain is in the medium pocket and part of it may extend toward the entrance of the pocket (i.e. toward the solvent). In binding mode II the orientation of propranolol is reversed (see Figs. 1 and S1 of the Supplementary data). Only conformations of the substrate were identified in which its hydroxyl group is close to the catalytic His224 and the acetylated serine. This explained the experimentally observed chemoselectivity of CalB. In addition, to check the reliability of the complexes identified by docking, they were subjected to short

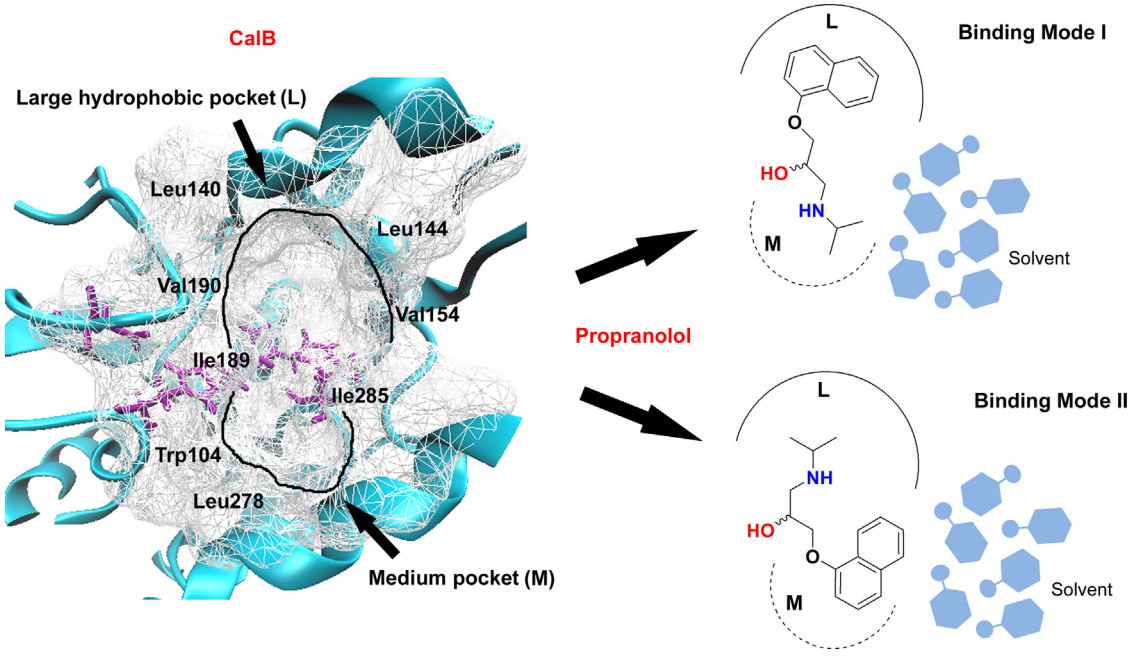

Fig. 1. Characteristic binding modes of propranolol in the CalB binding pocket. The structure of acetyl-CalB (AcCalB) is shown on the left with the catalytic triad Asp-His-Ser oriented from left to right. The binding pocket of CalB is constituted by a large hydrophobic pocket above the catalytic triad and a medium pocket below it. The large pocket is lined by Ile189 and Val190 on the left, Val154 on the far right, as well as Leu140 and Leu144 at the top. Deep in this pocket, Asp134 is on the left and Gln157 on the right. The medium pocket is below the catalytic Ser105 and is crowded by Trp104 below it and the Leu278–Ala287 helix (helix α10) to the right. In binding mode I (up to the right) the naphthoxy side chain of propranolol lies in the large hydrophobic pocket of CalB while its isopropylamine side chain in the medium pocket and may extends to toward the entrance of the binding pocket. Conversely, in binding mode II (down to the right) the former lies in the medium pocket and the latter in the large pocket.

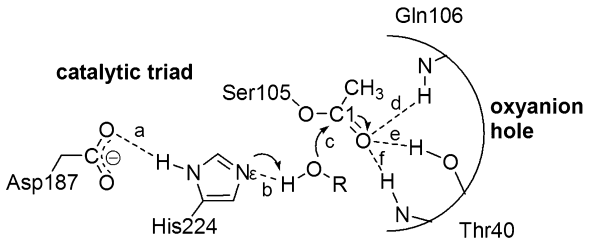

Scheme 2. Michaelis complexes (MCCs) between AcCalB and propranolol in the *O*-acetylation of propranolol catalyzed by CalB. a–f are the most important interatomic distances for the catalytic process. The acylated catalytic serine is referred to as SEA.

(100 ps) MD simulations in explicit toluene. Interestingly, a different temporal stability was observed for each complex, which is expected to play an important role for the enantioselectivity of the reaction [19].

With the aim to gain a deeper understanding of the molecular basis for the observed enantioselectivity in the CalB-catalyzed acetylation of (*R*,*S*)-propranolol, in the present study we perform a more extensive sampling of the MCCs of the deacylation step. Starting from the optimized Michaelis complexes between acetylated CalB (AcCalB) and propranolol obtained in our previous study by docking [18], multiple 1.5 ns MD simulations were carried out using different initial velocity distributions in order to improve the sampling of the conformational space [20–22]. The analysis of the MD trajectories was focused on the interatomic distances important for the catalytic process (see Scheme 2), the enzyme–substrate–solvent interactions involved in the binding modes of the substrate, the temporal stability (lifetime) of the reactive MCC complexes, and the ability of the propranolol enantiomers to form near attack conformations (NACs). NACs are conformers in which the atoms involved in the bond formation are at van der Waals distance and the angle of approach is ±15° of the angle of the bond formed in the transition state (TS). NACs are turnstiles through which the reactants must pass in order to reach the TS. A higher population of the NACs indicates a lower free energy change required to reach the NACs, thus the population of NACs is indicative of the reaction rate [23–26]. Thereby, based on the analysis of the MD trajectories, the reactivities of several conformations of both *R*- and *S*-propranolol were estimated and the enzyme–substrate interactions which are essential for the enantioselectivity were identified.

2. Experimental

In our previous study *R*- and *S*-propranolol were docked against acetylated CalB (AcCalB) [18]. The AcCalB structure used as target for the docking was prepared using the crystal structure of CalB (entry number 1TCA in the Protein Data Bank [27]) as starting point. This structure contains 286 crystal waters. During the docking procedure seven water molecules (HOH130, HOH136, HOH149, HOH219, HOH238, HOH265, HOH285) were removed from the active site cavity to accommodate the substrate, following similar studies on lipase-catalyzed reactions [28,29]. Three and four possible reactive complexes for *R*- and *S*-propranolol were identified, respectively. For *R*-propranolol, two complexes in binding mode I and one complex in binding mode II were found. These complexes are referred to as R1–R3, respectively. For *S*-propranolol we found three complexes in binding mode I and one complex in binding mode II. We refer to these complexes as S1–S4, respectively. These optimized complexes (including the remaining CalB crystal waters) were used as starting structures for 1.5 ns MD simulations in explicit toluene. They are shown in Section 1 of the Supplementary data. The remaining crystal waters are kept as they are important for the conservation of the enzyme structure in an active conformation [30].

The MD simulations were carried out using the CHARMM program (version 35b5) [31] in combination with the CHARMM22 force field [32,33]. For each complex three MD simulations with different initial velocity distributions were performed, corresponding to values of the random seed parameter iseed of 314159, 835 and 234. The MD simulations carried out using the iseed values 835 and 234 are indicated by * and ** respectively. Because there are no CHARMM force field parameters available for propranolol, a QM/MM MD approach was used. The QM region corresponding to *R*- or *S*-propranolol was treated by the self-consistent charge-density functional tight binding (SCC-DFTB) method [34] and the MM region (acetylated-CalB, toluene and crystal waters) by the CHARMM22 force field. All distances involving hydrogen atoms were constrained by SHAKE [35]. The nonbonded interactions were treated using group-based extended electrostatics [36]. In this approach, the electrostatic interactions between particles closer than a cutoff distance (14 Å in our case) are treated by the conventional pairwise additive scheme, while the interactions at larger distance are approximated by a computationally cheaper multipole approach.

The protein was placed in a solvent sphere of 40 Å radius containing 4454 toluene molecules cut out from an equilibrated simulation of toluene under periodic boundary conditions. This solvent sphere was centered at the alpha carbon of the acetylated catalytic serine (SEA:CA) and covered the entire complex (see Fig. S2 of the Supplementary data). All toluene molecules whose non-hydrogen atoms were within 2.8 Å of any existing non-hydrogen atom were deleted. An active region including all protein residues within 30 Å of the SEA:CA atom and the substrate was defined. All atoms of protein residues outside this active region were kept fixed during the MD simulations. Furthermore, to keep the shape of the solvent spherical and to prevent evaporation of solvent molecules in the MD simulations, toluene and water molecules were restrained by a quartic spherical boundary potential which is zero until 38.5 Å, has a shallow minimum of -0.25 kcal mol^{-1} at 39.5 Å and increases at larger distances (parameters FORCE = 0.2, P1 = 2.25, and DROFF = 38.5). Thereafter the toluene molecules within the sphere and the crystal waters were geometry-optimized, performing first 250 steps of steepest descent (SD) followed by 250 steps of adapted-basis Newton–Raphson minimization (ABNR), keeping all other atoms fixed. We performed two more minimizations of 250 steps each (SD and ABNR), optimizing the active region with the water and toluene molecules, applying a harmonic position restraint with force constant k = 30 mol Å^{-2} to the active region. Then a molecular dynamics simulation (15,000 steps) was performed increasing the temperature from 50 K to 300 K in steps of 10 K every 100 MD steps. The Verlet algorithm was used with a time step of 1 fs. This solvation procedure was repeated 12 times, and in the last two cycles the number of steps used in the dynamics was increased to 30,000. During the solvation procedure, harmonic positional restraints were applied to the atoms in the active region, which were successively lowered in each of the iterations. Finally, all constraints were removed and a production molecular dynamics simulation of 1.5 ns was run. Again, the temperature was raised from 50 K to 300 K in steps of 10 K every 100 MD steps. The system was equilibrated after 10 ps, so we used the remaining 1450 ps for analyses.

In these MD simulations the temporal stability of the AcCalB-propranolol complexes and their ability to lead to the formation of the second tetrahedral intermediate and then to acetyl-propranolol were checked. As a measure of the structural stability of the protein, the root mean square deviations (RMSD) with respect to the initial structure were calculated by superimposing all backbone heavy atoms of the protein. The MD trajectories were analyzed based on four criteria which have been successfully used in previous studies of lipase-catalyzed reactions for characterizing productive

binding modes (binding modes of the substrate which lead to formation of the product). These criteria are: (a) protein distortion, (b) hydrogen bond interactions between the acetate oxygen of the acetylated catalytic serine (SEA:O) and the residues of the oxyanion hole (distances **d-f** in Scheme 2), (c) the distance of the hydroxyl group of propranolol to the His224:Nε and SEA:C1 (carboxylic carbon of the acetylated catalytic serine) atoms (distances **b** and **c** in Scheme 2), (d) steric clashes with the enzyme [37–41]. Binding modes were considered as productive if all catalytically essential hydrogen bonds were maintained, the substrate avoided steric clashes with the enzyme, and its hydroxyl group was simultaneously positioned close to the catalytic residues His224 and SEA. The results of all MD simulations were analyzed using the program VMD [42].

3. Results and discussion

3.1. Protein distortion

1.5 ns MD simulations of the AcCalB-propranolol complexes were carried out. The RMSD value for all heavy atoms of the protein backbone with respect to the initial structure increased gradually during heating and equilibration time for the first 10 ps. After this phase a plateau with a RMSD value of about 1 Å is reached in all simulations (see Fig. S3 of the Supplementary data). The largest movements are observed in several surface loops (residues 250–267, 215–222, 1–12, 22–26, 67–75 and 170–178), a β-sheet constituting the C-terminal (residues 310–317), two short α-helix (α2: residues 44–49 and α5: residues 139–150), a long α-helix (α10: residues 267–289) and several residues constituting the binding pocket of CalB (residues 104, 154, 189, 190 and those making part of the α10 and α5 helix) (see Fig. S4 of the Supplementary data). This is in agreement with the results reported by other authors about the flexibility of CalB in organic solvents (e.g. chloroform, methanol and cyclohexane) and water [30,43,44]. In these studies it has also been reported that the regions with higher flexibility in CalB are the same in water and organic solvents and that only the degree of flexibility depends on the solvent [30]. On the other hand, the average RMSD values with respect to the crystal structure of the protein are about 0.90 Å and 1.22 Å (see Table S1 of the Supplementary data), which shows that the CalB structure is well conserved during the MD simulations. In particular the hydrogen bond interaction between Asp187 and His224 is maintained (see the next section) and the average distance between the SEA:Oγ and His224:Nε atoms is about 3.21–3.36 Å (see Table S2 of the Supplementary data), indicating that the disposition of the catalytic triad is stable during the simulations.

As found by Vallikivi et al. [39] for acetylation of prostaglandins, and as has successfully been used by other researches working with lipase catalyzed reactions [37,38], a RMSD value of <3 Å between the protein structures during the MD simulations and the CalB crystal structure was chosen as the limit to consider a complex to be in a productive binding mode. Because this criterion is satisfied in all simulations, all complexes formed during the MD simulations which satisfy the other three criteria mentioned above (see Section 2) may be considered productive complexes. Therefore, subsequent analysis of the MD simulations was focused on those criteria.

3.2. Hydrogen bonds between the catalytic residues

The MD trajectories of the AcCalB-propranolol complexes were first analyzed with respect to the orientation of the acetylated serine (SEA) in the oxyanion hole, in order to check if this residue preserves a catalytic configuration. The average distances **d-f** (see Scheme 2) for each complex in the MD simulations are given in the Table S3 of the Supplementary data. In all MD simulations the acetylated serine shows a similar behavior. The carbonyl oxygen (SEA:O) of the acetate points toward the oxyanion hole during the whole simulation. A strong hydrogen bond is formed between the SEA:O atom and the side chain–OH of the residue Thr40 (distance e in Scheme 2) with an average distance between 1.78 and 1.83 Å. The hydrogen bonds between the SEA:O atom and the —NH functions of the residues Gln106 and Thr40 (distances **d-f** in Scheme 2) have average distances of 2.12–2.26 Å and 2.02–2.44 Å respectively. In general, the hydrogen bonds with the oxyanion hole are stable throughout the MD simulations of all complexes. There are only short periods (less than 2% of the total simulation time in most of the MD simulations) in which mainly the SEA:O-Thr40:NH hydrogen bond (distance **f** in Scheme 2) is disrupted due to the conformational changes of the substrate during the MD simulations. Thus at least two of the hydrogen bonds with the oxyanion hole are formed throughout the MD trajectory. See Figs. S5–S10 of the Supplementary data.

The hydrogen bond between the catalytic residues Asp187 and His224 (distance **a** in Scheme 2) has an average distance between 1.90 and 2.06 Å and is stable throughout the MD simulations of all complexes (see Table S3 and Figs. S5–S10 of the Supplementary data). This hydrogen bond is also important for the catalytic process as this interaction increases the basicity of the catalytic histidine, such that proton abstraction from the hydroxyl group of propranolol becomes likely, facilitating the nucleophilic attack on the carbonyl group of the acetylated serine (SEA).

The stability of these hydrogen bonds throughout all the simulations suggests that neither the orientation of the acetyl group toward the oxyanion hole nor the catalytic role of the residue Asp187 are determining factors for the formation of reactive complexes between AcCalB and *R*- or *S*-propranolol and thus for the enantioselectivity of the reaction. Instead the enantioselectivity of the reaction mainly depends on the ability of the propranolol enantiomers to adopt conformations inside the binding pocket of CalB which are suitable for a reaction and on the difference of the reactivities of these conformations.

3.3. The nucleophilic attack

As explained in Section 2, for considering a complex as productive the hydroxyl group of propranolol has to be positioned simultaneously close to the His224:Nε and SEA:C1 atoms and steric contacts with the protein must not be observed. We decided to use a maximal value of 4 Å for the distances **b** and **c** (see Scheme 2), following other authors studying lipase-catalyzed acetylation reactions [37,38,40]. Several conformers satisfying these distance criteria were identified for *R*- and *S*-propranolol, which exhibit H–H contact distances with the protein which are longer than 2.6 Å (i.e. no steric clashes are observed). Thus several reactive conformers were identified for both *R*- and *S*-propranolol. The reactivities of these conformers are analyzed below in terms of the distances **b** and **c**, the enzyme–substrate interactions, the temporal stability and the formation of NACs.

3.3.1. AcCalB-propranolol complexes in binding mode I

In most of the MD simulations of the AcCalB-propranolol complexes in binding mode I propranolol is stabilized with its hydroxyl group close to the catalytic residues only during some time of the MD trajectories (see details below). Then the substrate undergoes conformational changes leading to non-productive complexes or movement of propranolol from the binding pocket to the solvent. The stabilization of propranolol close to the catalytic residues is mediated mainly by CH-π interactions established between its naphthyl group and the aliphatic side chains of the residues at the large pocket of CalB (Ile189, Ala141, Leu144, Val154 and

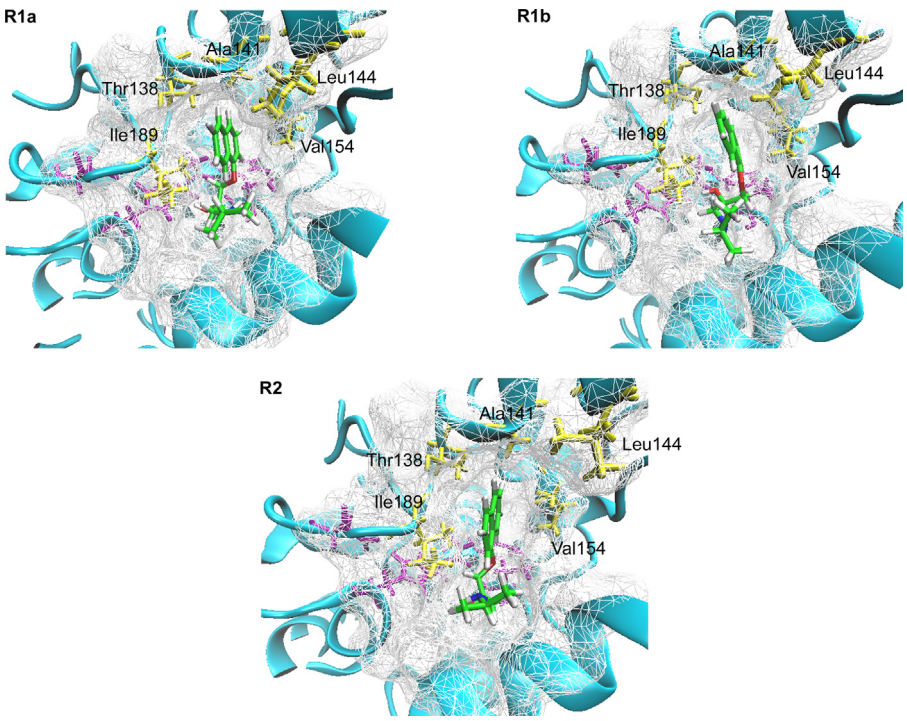

Fig. 2. Predominant conformations of *R*-propranolol in the MD simulations of the Michaelis complexes between AcCalB and *R*-propranolol in binding mode I. R1a and R1b correspond to the major reactive conformers of *R*-propranolol observed in the MD simulations of the complex R1. The catalytic triad (Asp187, His224 and acetylated Ser105) and the oxyanion hole (Thr40 and Gln106) are shown in purple. The residues constituting the binding pocket of CalB are shown in wireframe representation (gray). The most important residues contributing to the stabilization of propranolol by CH-π interactions are shown in yellow. (For interpretation of the references to color in this figure legend, the reader is referred to the web version of the article.)

Thr138) (see Figs. 2 and 4). On the other hand, the destabilization of the complexes is mainly due to hydrophobic interactions established between the isopropyl side chain of propranolol and the solvent (toluene) during the simulations, which leads to the loss of the hydrophobic interactions between the isopropyl side chain of propranolol and the side chains of the residues at the medium pocket (Leu278, Ala281, Ala282, Ile285). Because the binding pocket of CalB is accessible to the solvent and in binding mode I the isopropyl side chain of propranolol may extends toward the entrance of the binding pocket, propranolol interacts continuously with toluene, leading to the loss of the CH-π interactions between the naphthyl group of propranolol and the residues at the large pocket. Thereby, as described in the following sections, it is found that the better exposition of the isopropyl group of propranolol toward the entrance of the binding pocket the shorter the temporal stability of propranolol close to the catalytic residues (thus of the reactive complexes) in binding mode I.

3.3.1.1. R-propranolol complexes in binding mode I. The MD simulations of the *R*-propranolol complexes in binding mode I were carried out using two initial structures corresponding to the complexes R1 and R2 (see Fig. S1 of the Supplementary data). In these structures the naphthyl group of propranolol is positioned in the same plane, but pointing toward the exterior of the binding pocket of CalB in R1 and toward the interior of the binding pocket in R2. Propranolol is near to the catalytic residues (SEA and His224) for a longer time in the simulations of R1 (more than 200 ps) than in the simulations of R2 (less than 5 ps). This is attributed to the better ability of the solvent to interact with the isopropyl group of propranolol in the system R2, as this isopropyl group is more exposed toward the exterior of the binding pocket in this system

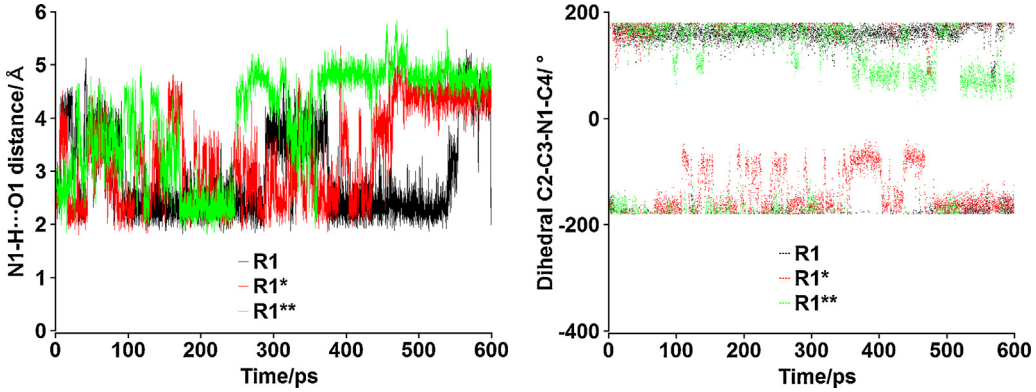

Fig. 3. Time evolution of the N1—H···O1 intramolecular hydrogen bond and the C2—C3—N1—C4 dihedral angle of propranolol in the MD simulations of the complex R1. Only the first 600 ps of the simulations are shown. Simulations with different initial velocities are indicated by *.

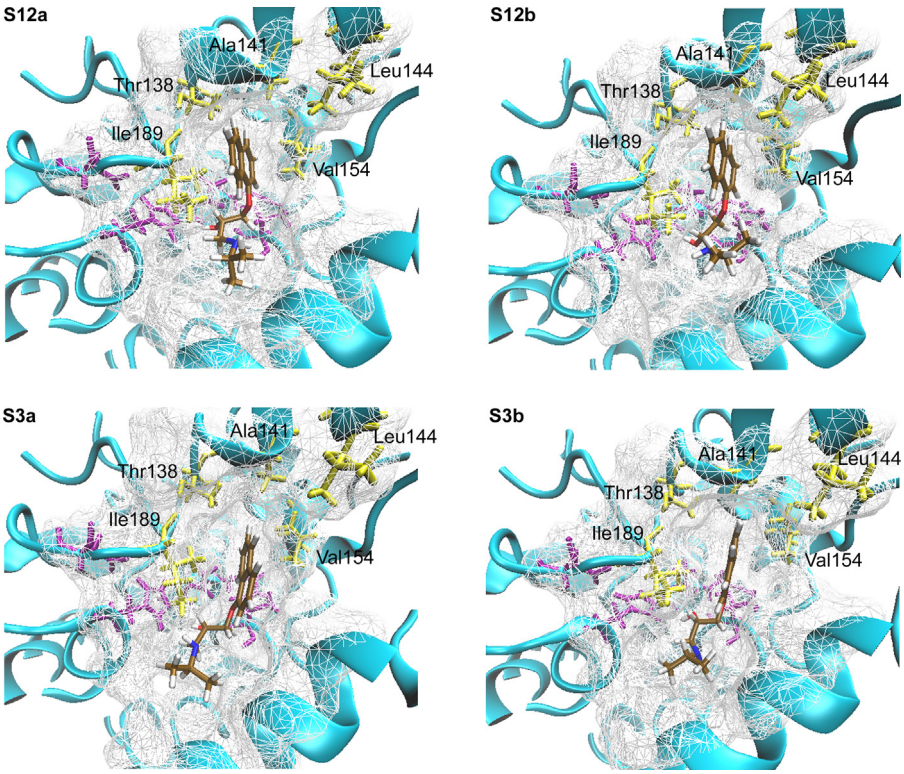

Fig. 4. Predominant reactive conformations of *S*-propranolol in the MD simulations of the Michaelis complexes between AcCalB and *S*-propranolol in binding mode I. The catalytic triad (Asp187, His224 and acetylated Ser105) and the oxyanion hole (Thr40 and Gln106) are shown in purple. The residues constituting the binding pocket of CalB are shown in wireframe representation (gray). The most important residues contributing to the stabilization of propranolol by CH-π interactions are shown in yellow. (For interpretation of the references to color in this figure legend, the reader is referred to the web version of the article.)

(see section 4.1 of the Supplementary data for details). The predominant conformations of *R*-propranolol in the MD simulations of these complexes are shown in Fig. 2. The observed interaction between propranolol and the solvent in R2 does not permit the formation of reactive complexes and only for R1 reactive complexes are found (**R1a** and **R1b**). **R1a** is characterized by the formation of an intramolecular hydrogen bond between the amino and ether groups of propranolol (N1—H···O1). The average distance of this hydrogen bond is 2.43 ± 0.06 Å (see Fig. 3). **R1b** is similar to **R1a**, but in this conformer the N1—H···O1 intramolecular hydrogen bond is not formed due to the orientation of the isopropylamine side chain. Propranolol is switching between **R1a** and **R1b** while it is close to the catalytic residues, by rotation of the C2—C3—N1—C4 dihedral angle (see Fig. 3).

The average distances **b** and **c** for **R1a** and **R1b** are given in Table 1. It can be seen that the distance **c** is similar for both conformers, while the distance **b** is remarkably shorter for **R1a** compared to **R1b**. This shows that **R1a** is more accessible to be acylated by the enzyme, as a stronger hydrogen bond interaction with His224 (distance **b**) increases the nucleophilicity of the alcohol oxygen. Visual inspection shows that this behavior is strongly related to the folding of the propranolol structure due to the formation of the N1—H···O1 intramolecular hydrogen bond.

The average distances corresponding to the CH-π interactions stabilizing the reactive conformers of *R*-propranolol in binding mode I are shown in Table 2. Because of their linearity the CH-π interactions between the naphthyl group of propranolol and the side chains of the residues Ile189, Val154 and Leu144 are expected to be stronger [45]. The side chains of these residues are pointing toward the center of the naphthyl rings, especially the side chain of Ile189. Thus Ile189 is expected to have a large contribution to the stabilization of the TS involved in the transformation of the *R*-propranolol in binding mode I (see the next section).

3.3.1.2. S-propranolol complexes in binding mode I. The MD simulations of the *S*-propranolol complexes in binding mode I were carried out using three initial structures corresponding to the complexes S1, S2 and S3 (see Fig. S1 of the Supplementary data). In S1 and S2 the naphthyl group of propranolol is oriented pointing toward the exterior of the binding pocket while in S3 it is oriented pointing toward the interior of the binding pocket. In general, propranolol is located near to the catalytic residues for a longer period of time in the simulations of S3 (more than 1300 ps) than in simulations of S2 and S1 (less than 600 ps). This behavior observed for *S*-propranolol in binding mode I differs from that of *R*-propranolol, which is stabilized close to the catalytic residues for a longer time in the system in which its naphthyl group is oriented pointing toward the exterior of the binding pocket (R1). This is explained by a better exposition of the isopropyl group of propranolol toward the exterior of the binding pocket (facilitating the interaction with the solvent) in systems S1 and S2 than in S3. This contrasts with what is observed in R1 and R2, respectively. Details are given in the Section 4.2 of the Supplementary data.

The predominant conformations of *S*-propranolol in the MD simulations of these complexes are shown in Fig. 4. In all MD simulations propranolol is able to form reactive complexes. As in the case of *R*-propranolol, when the naphthyl group of *S*-propranolol is oriented pointing toward the exterior of the binding pocket (complexes S1 and S2), propranolol switches between two reactive conformations during the MD simulations. These conformations are generated by rotation of the same C2—C3—N1—C4 dihedral angle, and differ by a N1—H···O1 intramolecular hydrogen bond. As this behavior is observed in the MD simulations of S1 and S2, we refer to these two conformations as **S12a** and **S12b**, **S12a** being the conformation in which the N1—H···O1 hydrogen bond is present. The average distance of this hydrogen bond is 2.46 ± 0.09 Å, which is close to the value obtained for **R1a**. A similar behavior

Table 1
Average distances[a] (in Å) between the hydroxyl group of propranolol and the carbonyl carbon of the acetylated serine and the Nε atom of the catalytic histidine in the MD simulations[b] of the Michaelis complexes between AcCalB and *R*- or *S*-propranolol in binding mode I.

Complex	Distance					
	b	**c**	**b***	**c***	**b****	**c****
R1a	2.31 (0.30)	3.77 (0.17)	2.26 (0.38)	3.67 (0.21)	2.25 (0.31)	3.71 (0.17)
R1b	2.86 (0.40)	3.60 (0.21)	3.06 (0.45)	3.70 (0.12)	2.70 (0.47)	3.61 (0.21)
S12a[c]	2.47 (0.42)	3.61 (0.22)	2.31 (0.48)	3.60 (0.23)	2.22 (0.37)	3.49 (0.26)
S12b[c]	2.38 (0.29)	3.71 (0.24)	2.28 (0.44)	3.51 (0.29)	2.27 (0.38)	3.49 (0.24)
S3a	2.15 (0.31)	3.28 (0.21)	2.19 (0.30)	3.63 (0.24)	2.29 (0.35)	3.42 (0.23)
S3b	2.18 (0.35)	3.25 (0.20)	2.18 (0.28)	3.28 (0.23)	2.20 (0.31)	3.37 (0.22)

[a] Distances **b** and **c** correspond to those shown in the Scheme 2. Only periods during which the distances **b** and **c** were simultaneously less than 4 Å were taken into account. Numbers in brackets correspond to standard deviations from average values.
[b] MD simulations with different initial velocity distribution are indicated by *.
[c] Averages have been performed over the MD simulations of S1 and S2.

Table 2
Average distances[a] (in Å) of the interactions between the carbon atoms[b] of the naphthyl rings of propranolol and the residues of the binding pocket of the surrounding protein, in the MD simulations of the Michaelis complexes between AcCalB and *R*- or *S*-propranolol in binding mode I.

Non polar interactions	Complex					
	R1a	R1b	S12a	S12b	S3a	S3b
Val154 Cγ2···C2′	4.27 (0.08)	4.20 (0.06)	4.26 (0.14)	4.32 (0.25)		
Val154 Cγ2···C7′					4.22 (0.03)	4.22 (0.05)
Val154 Cγ1···C3′	4.10 (0.07)	4.08 (0.04)	3.90 (0.03)	4.00 (0.11)		
Val154 Cγ1···C4′	4.24 (0.33)	4.21 (0.38)	3.78 (0.04)	3.71 (0.05)		
Val154 Cγ1···C10′	4.37 (0.12)	4.33 (0.08)	4.38 (0.04)	4.27 (0.10)	4.54 (0.16)	4.64 (0.01)
Val154 Cγ1···C5′					3.97 (0.07)	4.02 (0.02)
Val154 Cγ1···C6′					3.68 (0.03)	3.70 (0.04)
Leu144 Cδ1···C5′	4.18 (0.16)	4.15 (0.11)	4.00 (0.10)	4.14 (0.16)		
Leu144 Cδ1···C6′	3.88 (0.09)	3.85 (0.06)	3.96 (0.22)	4.00 (0.22)		
Ala141 Cβ···C5′	3.99 (0.06)	3.99 (0.06)	4.14 (0.17)	4.22 (0.06)	4.21 (0.17)	4.35 (0.13)
Thr138 Cγ2···C4′	4.05 (0.08)	3.99 (0.03)	3.93 (0.21)	3.98 (0.23)		
Thr138 Cγ2···C6′					3.82 (0.11)	3.87 (0.06)
Ile189 Cγ2···C10′	3.92 (0.07)	3.88 (0.06)	4.09 (0.06)	4.10 (0.11)	3.96 (0.00)	3.97 (0.03)
Ile189 Cγ2···C9′	3.76 (0.05)	3.74 (0.05)	3.66 (0.04)	3.66 (0.09)	3.79 (0.05)	3.73 (0.01)

[a] Averages have been performed over the three MD simulations with different seed velocities. Numbers in brackets correspond to standard deviations from average values.
[b] Labels for the carbon atoms of propranolol are given in Scheme 1.

is observed in the simulations of S3, where two major reactive conformers of propranolol are observed (**S3a** and **S3b**) differing in the C2—C3—N1—C4 dihedral angle, but without formation of a N1—H···O1 intramolecular hydrogen bond. This hydrogen bond cannot be formed because the oxygen atom O1 is positioned far from the amino group (N1—H) when the naphthyl group of propranolol is oriented pointing toward the interior of the binding pocket.

The average distances **b** and **c** for the reactive complexes of *S*-propranolol in binding mode I are also shown in Table 1. These complexes present a different dynamic behavior compared to the *R*-propranolol complexes. Reactive complexes of *S*-propranolol in which the naphthyl group is oriented pointing toward the exterior of the binding pocket (**S12a** and **S12b**) present a similar ability to be transformed by the enzyme, as in these complexes the hydroxyl group of propranolol is simultaneously positioned near to His224 and SEA at similar distances. Furthermore, the *S*-enantiomer is also able to form reactive complexes when its naphthyl group is oriented pointing toward the interior of the binding pocket, which is not the case for *R*-propranolol, due to the destabilization of the corresponding complex (R2) by the solvent (see the previous section).

The hydroxyl group of propranolol is closer to the catalytic residues in the *S*-propranolol complexes than in the *R*-propranolol complexes, especially in comparison to the **R1b** complex. This means that in binding mode I *S*-propranolol fits into the CalB binding pocket in conformations in which its hydroxyl group is in a better position to be acetylated by CalB than the *R*-propranolol. This suggests a faster transformation of the *S*-propranolol over *R*-propranolol. However, analysis of the CH-π interactions contributing to the stabilization of the reactive *S*-propranolol conformers shows that these conformers are more weakly stabilized by this type of interaction (according to the average distances and standard deviations, and to the linearity of the interactions) in comparison to the reactive *R*-propranolol conformers (see Table 2). This suggests a better stabilization of the TS involved in the transformation of the *R*-enantiomer, which would enhance the reactivity of this enantiomer. Particularly it should be noted that **S3a** and **S3b** loose the interaction with Leu144 (see Fig. 4). Furthermore, as is reflected in the average distances and standard deviations, **R1a** and **R1b** are more strongly stabilized by the residues Leu144, Ala141, Thr138 and Ile189 in comparison to **S12a** and **S12b**. For example, the average distances between the atom Cγ2 of Ile189 and the atoms C10′ and C9′ of propranolol are 3.92 ± 0.07 Å and 3.76 ± 0.05 Å in case of **R1a**, while in case of **S12a** (specular binding mode of **R1a**) are 4.09 ± 0.06 Å and 3.66 ± 0.04 Å, respectively. The average distance between the atom Cβ of Ala141 and the atom C5′ of propranolol is 3.99 ± 0.06 Å in case of **R1a**, while in case of **S12a** it is 4.14 ± 0.17 Å. Finally, the average distance between the atom Cδ1 of Leu144 and the atom C6′ of propranolol, which is 3.88 ± 0.09 Å for **R1a** and 3.96 ± 0.22 Å for **S12a**.

Several studies have been reported showing experimental and theoretical evidence of a major stabilization of the transition state involved in the transformation of the faster enantiomer by hydrophobic interactions. One example is the resolution of methyl (±)-3-hydroxypentanoate catalyzed by *C. antarctica* lipase B using ammonia and benzyl amine as nucleophiles. Molecular dynamics simulations carried out over the second tetrahedral intermediate revealed that the higher number of contacts involving non-polar atoms of both the acyl chain (substrate) and some of the residues

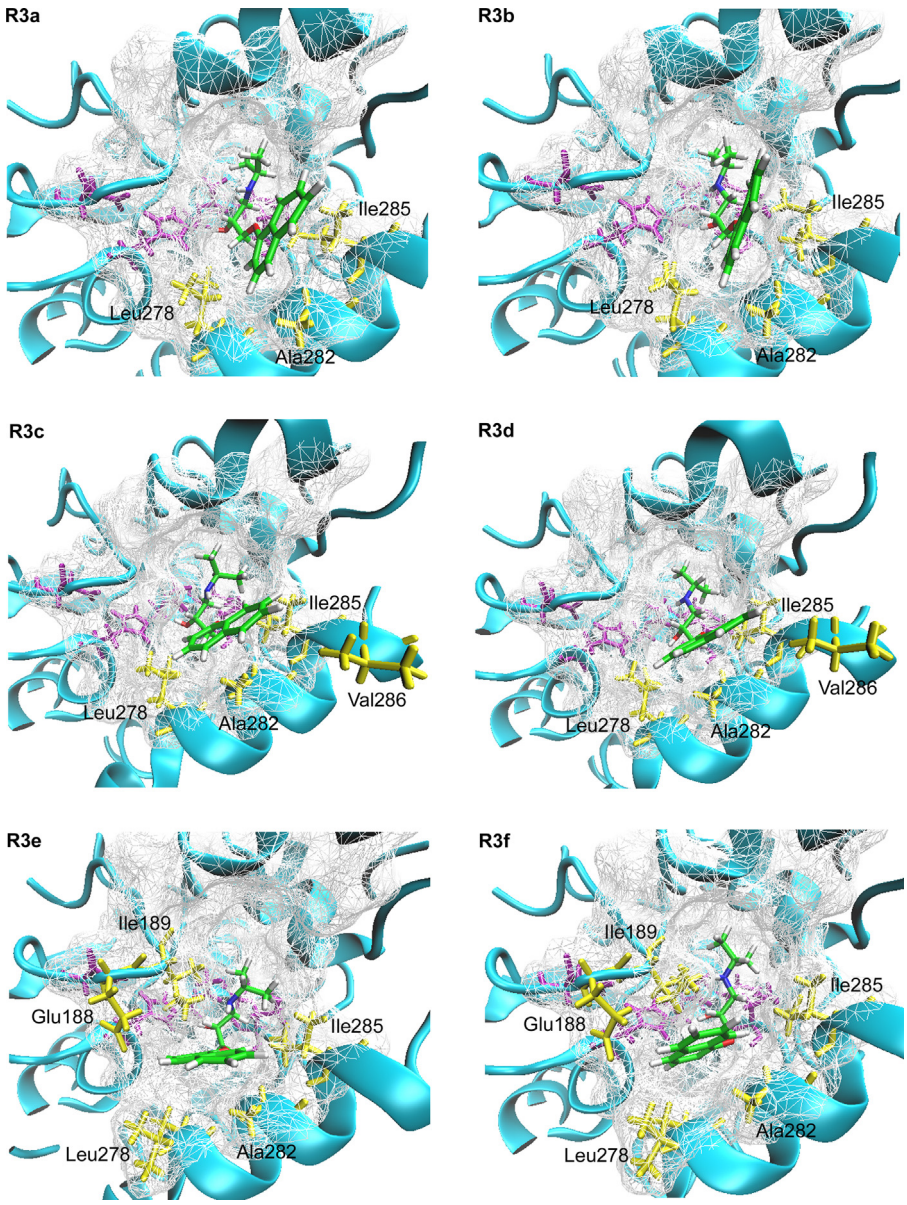

Fig. 5. Predominant reactive conformations of *R*-propranolol in the MD simulations of the Michaelis complexes between AcCalB and *R*-propranolol in binding mode II. The catalytic triad (Asp187, His224 and acetylated Ser105) and the oxyanion hole (Thr40 and Gln106) are shown in purple. The residues constituting the binding pocket of CalB are shown in wireframe representation (gray). The most important residues contributing to the stabilization of propranolol by CH-π interactions are shown in yellow. (For interpretation of the references to color in this figure legend, the reader is referred to the web version of the article.)

of the CalB binding pocket (including Ile189) are responsible for the higher enantioselectivity observed in the aminolysis reaction [46]. Another good example showing specifically the contribution of the CH-π interactions to the enantioselectivity is the improvement of the catalytic activity and enantioselectivity of *Burkholderia cepacia* toward secondary alcohols through the I287F/I290A double mutation. Substrate mapping analysis strongly suggested that Phe287 contributes to enhancement the reactivity of the *R*-enantiomer by a CH-π interaction with the substrate, of which the estimated energy was $-0.4\,\text{kcal mol}^{-1}$ [47]. The CH-π interactions have also shown to be responsible for the enantioselectivity observed in other reactions such as the transfer hydrogenation of aromatic carbonyl compounds catalyzed by chiral n^6-Arene-Ruthenium (II) complexes [48].

3.3.2. AcCalB-propranolol complexes in binding mode II

In contrast to binding mode I, in the MD simulations of the AcCalB-propranolol complexes in binding mode II the substrate never leaves the binding pocket. This is because in this binding mode the solvent interacts mainly with the naphthyl group of propranolol, which is strongly stabilized by CH-π interactions with the residues at the medium pocket of CalB (Ile285, Val286, Ala282 and Leu278, see Figs. 5 and 6). As the strength of a CH-interaction depends on its linearity [45], the temporal stabilization of propranolol (in binding mode II) with its hydroxyl group close to the catalytic residues depends on the orientation of its naphthyl group in the medium pocket. Generally speaking, the better the stabilization of the naphthyl rings by the residues of the surrounding protein and the less exposed they are to the solvent, the longer the temporal stability of propranolol close to the catalytic residues (thus of the reactive complexes) in binding mode II (see Section 4.3 of the Supplementary data for details).

3.3.2.1. R-propranolol complexes in binding mode II. In the MD simulations of R3 a total of six reactive complexes of *R*-propranolol are found (**R3a–R3f** in Fig. 5). Interestingly, not all complexes are

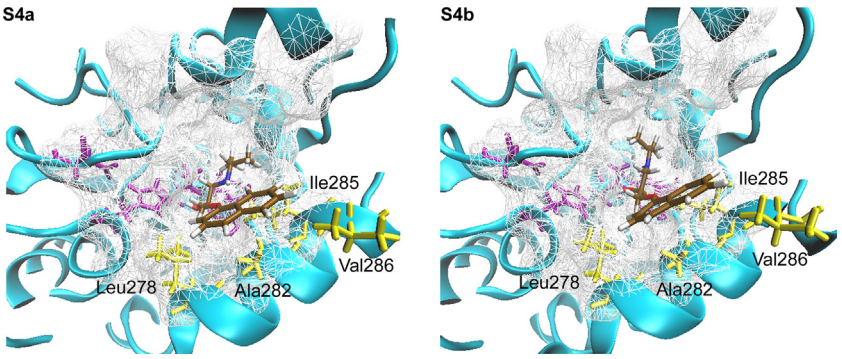

Fig. 6. Predominant reactive conformations of *S*-propranolol in the MD simulations of the Michaelis complexes between AcCalB and *S*-propranolol in binding mode II. The catalytic triad (Asp187, His224 and acetylated Ser105) and the oxyanion hole (Thr40 and Gln106) are shown in purple. The residues constituting the binding pocket of CalB are shown in wireframe representation (gray). The most important residues contributing to the stabilization of propranolol by CH-π interactions are shown in yellow. (For interpretation of the references to color in this figure legend, the reader is referred to the web version of the article.)

observed in all MD simulations, except **R3a** and **R3b**. **R3c** and **R3d** occur in two of the three MD simulations while **R3e** and **R3f** only in one MD simulation. These results show the versatility of using multiple MD simulations with different initial velocity distributions for sampling the conformational space in this type of systems. See Section 4.3 of the Supplementary data for details.

Similar to the simulations of the complexes in binding mode I, a rotation of the C2—C3—N1—C14 dihedral angle of propranolol is observed, resulting in a temporal formation of the N1—H···O1 intramolecular hydrogen bond. **R3a**, **R3c** and **R3e** are characterized by the formation of this hydrogen bond, with an average distance of 2.60 ± 0.21 Å, 2.41 ± 0.07 Å and 2.47 ± 0.24 Å, respectively. The main difference between these complexes is the orientation of the naphthyl group of propranolol in the medium pocket of CalB. **R3c** is generated from **R3a** by the simultaneous rotation of the O1—C1—C2—C3 and C1′—O1—C1—C2 dihedral angles, from $44 \pm 6°$ to $57 \pm 1°$ and from $139 \pm 0.3°$ to $102 \pm 0.9°$, respectively. These rotations move the naphthyl group of propranolol from a plane almost perpendicular to the Leu278-Ala287 helix (helix α10) in **R3a** to an orientation parallel to this helix in **R3c**. In turn **R3e** is generated from **R3c** by the simultaneous rotations of the same dihedral angles, from $57 \pm 1°$ to $79 \pm 9°$ and from $102 \pm 0.9°$ to $69 \pm 11°$, respectively. These rotations move the naphthyl group of propranolol toward the interior of the medium pocket. **R3b**, **R3d** and **R3f** are structural analogs of **R3a**, **R3c** and **R3e**, respectively. They only differ in the orientation of the amino group of propranolol, which does not favor the formation of the N1—H···O1 hydrogen bond in **R3b**, **R3d** and **R3f**.

The average distances **b** and **c** for the reactive complexes of *R*-propranolol in binding mode II are given in Table 3. In the complexes **R3a–R3d** the hydroxyl group of propranolol is simultaneously positioned closer to the catalytic residues when the N1—H···O1 intramolecular hydrogen bond is formed. While in **R3e** and **R3f** the hydroxyl group is positioned at a similar distance, suggesting that these complexes have the same ability to be acetylated by CalB. In general, the distances **b** and **c** in **R3e** and **R3f** are shorter than the ones observed in **R3a–R3d**. Furthermore, even though **R3e** and **R3f** are only found in one of the MD simulations, they are temporally more stable than the other *R*-propranolol conformers (more than 500 ps; see Table 4 and Section 4.3 of the Supplementary data). This is attributed to the higher number of protein residues contributing to the stabilization of these conformers through CH-π interactions as well as to a reduced exposition of the naphthyl group of propranolol to the solvent. In **R3a–R3d** propranolol is mainly stabilized through CH-π interactions between their naphthyl rings and the residues Ile285, Ala282, Leu278 and Val286, while in **R3e** and **R3f** it is also stabilized by the residues Ile189 and Glu188 as shown in Fig. 5 (see also Table S4 of the Supplementary data for details). The larger number of CH-π interactions contributing to the stabilization of these conformers may also play an important role in stabilizing the corresponding transition states. Thus these results suggest that the acetylation of **R3e** and **R3f** by CalB is favored compared to the other *R*-propranolol conformers.

3.3.2.2. S-propranolol complexes in binding mode II. In the MD simulations of S4 two reactive complexes of *S*-propranolol could be identified (**S4a** and **S4b** in Fig. 6). **S4a** and **S4b** are specular binding modes of **R3c** and **R3d**, respectively. They are also stabilized in the binding pocket of CalB by the residues Ile285, Ala282, Leu278 and Val286 by CH-π interactions. **S4a** and **S4b** differ in the orientation of their amino group, which forms an N1—H···O1 hydrogen bond only in **S4a**. This hydrogen bond is stronger than in the other reactive conformers of *R*- and *S*-propranolol, with an average distance of 2.29 ± 0.03 Å.

The average distances **b** and **c** of the **S4a** and **S4b** complexes are shorter than in the **R3a–R3d** complexes (see Table 3). According to this, the transformation of **S4a** and **S4b** is favored over **R3a–R3d**. In contrast, in terms of these distances, **R3e** and **R3f** display a similar ability to **S4a** and **S4b** to be acetylated by CalB. However, as observed in the complexes in binding mode I, the reactive conformers of *R*-propranolol are more strongly stabilized (by CH-π interactions with the surrounding protein residues) than the reactive conformers of *S*-propranolol in binding mode II (see Table S4 of the Supplementary data). For example, it can be seen in Figs. 5 and 6 that **R3e** and **R3f** are stabilized by a larger number of CH-π interactions than **S4a** and **S4b**. This suggests that these interactions are also responsible for a better stabilization of the transition states involved in the transformation of the *R*-propranolol complexes in binding mode II, leading to a faster transformation of this enantiomer, which would explain the experimentally observed enantioselectivity.

It is important to note that from the MD simulations of the Michaelis complexes between AcCalB and propranolol we cannot quantitatively estimate the contribution of the hydrophobic interactions between the substrate and CalB to the stabilization of the corresponding transition states, and therefore to the enantioselectivity. However, at least a qualitative idea is obtained, which may help to improve the enantioselective synthesis of propranolol through a rational redesign of CalB. The actual contribution of these interactions to the stabilization of the TS can be estimated from hybrid quantum chemical/molecular mechanical (QM/MM) calculations [49]. We are currently carrying out these calculations. The results will be published in a separate paper.

Table 3
Average distances[a] (in Å) between the hydroxyl group of propranolol and the carbonyl carbon of the acetylated serine and the Nε atom of the catalytic histidine in the MD simulations[b] of the Michaelis complexes between AcCalB and *R*- or *S*-propranolol in binding mode II.

Complex	Distance					
	b	**c**	**b***	**c***	**b****	**c****
R3a	2.87 (0.33)	3.55 (0.21)	2.82 (0.69)	3.63 (0.27)	2.69 (0.56)	3.69 (0.21)
R3b	2.81 (0.41)	3.61 (0.19)	3.11 (0.52)	3.74 (0.21)	3.08 (0.56)	3.65 (0.21)
R3c			2.74 (0.51)	3.70 (0.18)	2.34 (0.46)	3.60 (0.24)
R3d			3.11 (0.57)	3.76 (0.19)	2.99 (0.54)	3.76 (0.21)
R3e					2.20 (0.36)	3.43 (0.24)
R3f					2.39 (0.40)	3.15 (0.21)
S4a	2.18 (0.34)	3.28 (0.21)	2.18 (0.28)	3.62 (0.23)	2.28 (0.35)	3.41 (0.23)
S4b	2.14 (0.31)	3.24 (0.20)	2.18 (0.29)	3.45 (0.30)	2.23 (0.32)	3.39 (0.22)

[a] Distances **b** and **c** correspond to those shown in the Scheme 2. Only periods during which the distances **b** and **c** were simultaneously less than 4 Å were taken into account. Numbers in brackets correspond to standard deviations from average values.
[b] MD simulations with different initial velocity distribution are indicated by *.

Table 4
Lifetime and percentage of NACs[a] of each reactive conformer of *R*- and *S*-propranolol in the MD simulations of the AcCalB-propranolol complexes carried out with the third initial velocity distribution.

Binding mode I			Binding mode II		
Conformer	Lifetime** (ps)	NACs** (%)	Conformer	Lifetime** (ps)	NACs** (%)
R1a	116.7	0.09	R3a	9.5	1.05
R1b	118.4	1.18	R3b	24.5	0.41
S12a[b]	372.5	4.00	R3c	38.7	0.78
S12b[b]	715.8	13.90	R3d	214.4	0.05
S3a	1024.9	13.01	R3e	520.6	26.89
S3b	465.1	21.29	R3f	679.4	36.74
			S4a	577.4	1.52
			S4b	912.6	1.89

[a] The percentage of NACs formation is given related to the lifetime of each reactive conformer.
[b] Averages have been calculated over the MD simulations of S1 and S2 (see Section 3.3.1.2).

3.3.3. *Formation of near attack conformers (NACs)*

Finally we analyze the ability of the reactive conformers of propranolol to form near attack conformers (NACs). Because the reactants must pass through the NACs in order to reach the TS, the population of NACs is an indicative of the reaction rate [23]. We defined the NACs for the AcCalB-propranolol complexes as those in which the distances **b** and **c** are simultaneously ≤2.7 Å and ≤3.2 Å, respectively. We analyzed the fraction of the lifetime of each reactive conformer of propranolol in which NACs are formed during the MD simulations. All reactive conformers are able to form NACs and thus will reach the TS. The percentage of NACs of the two propranolol enantiomers is similar in all MD simulations with different initial velocity distributions. Therefore only the results of the analysis of the MD simulations with the third initial velocity distribution (iseed 234) are shown in Table 4. In this simulation all reactive propranolol conformers are present. It can be seen that in binding mode I the reactive conformers of *S*-propranolol occur more frequently and have a better ability to form NACs than the reactive conformers of *R*-propranolol. The lifetime of the reactive conformers of *R*-propranolol is <120 ps and the percentage of NACs is <2%, while for the reactive conformers of *S*-propranolol the lifetime is >300 ps and the percentage NACs is >4%. In contrast, in binding mode II, the percentage of NACs in the reactive complexes of *S*-propranolol is higher than in the **R3a–R3d** complexes but lower than in the **R3e** and **R3f** complexes. This is explained by the strong binding of propranolol to the active site of CalB in the **R3e** and **R3f** complexes (see Section 4.3 of the Supplementary data). The percentage of NACs in these complexes is higher than in the other complexes. This means that this stage of the reaction is kinetically favored for *R*-propranolol, which is in agreement with the experimental results. The moderate enantioselectivity of CalB may be partly attributed to the high percentage of NACs formation observed for the *S*-propranolol. See Tables S5 and S6 of the Supplementary data for details on the other simulations.

4. Summary and conclusions

In this work, the dynamic behavior of the Michaelis complexes of the deacylation reaction of the *O*-acetylation of propranolol catalyzed by CalB has been studied by multiple molecular dynamics simulations in explicit toluene. The analysis of the MD trajectories shows that different reactive conformations of *R*- and *S*-propranolol exist, which may be transformed to the corresponding second tetrahedral intermediate. These reactive conformations differ in their temporal stability and ability to reach the corresponding transition states. In binding mode I, the reactive conformers of *S*-propranolol are temporally more stable and have a better ability to form NACs than those of *R*-propranolol. On the other hand, in binding mode II, reactive conformers of *R*-propranolol are identified, which have a better ability to form NACs than all reactive *S*-propranolol conformers (either in binding mode I or II). This explains the preference of CalB to transform *R*-propranolol. The moderate enantioselectivity of CalB is explained by the frequency of NACs observed for several reactive *S*-propranolol conformers, which is just slightly lower than the frequency of NACs for the *R*-propranolol conformers.

The CH-π interactions established between the naphthyl group of propranolol and the surrounding protein residues are the major source of the stabilization of propranolol with its hydroxyl group near to the catalytic residues. These interactions are in general stronger in the reactive complexes of *R*-propranolol than in those of *S*-propranolol. Thus these interactions are expected to play an important role in stabilizing the corresponding transition states involved in the transformation of the *R*-propranolol, enhancing the reactivity of this enantiomer. Based on the strength of their interactions with the naphthyl group of *R*-propranolol, Ile189, Ala282 and Leu278 have been identified as key residues for the enantioselectivity of CalB. Ile189 is particularly important as this residue is involved in CH-π interactions with *R*-propranolol both in binding mode I and II. These results suggest key residues for improving

the enantioselective acylation of propranolol catalyzed by CalB, through the rational redesign of CalB.

Acknowledgements

This work was supported by Grant No. 110256933409 from COLCIENCIAS and VIE-UIS (Project 5702). The support of COLCIENCIAS to A.M. Escorcia (PhD Program Fellowship 2009) is gratefully recognized.

Appendix A. Supplementary data

Supplementary material related to this article can be found, in the online version, at http://dx.doi.org/10.1016/j.molcatb.2014.06.010.

References

[1] A.M. Barret, J. Pharmacol. 16 (1985) 95–108.
[2] R. Rabkin, D.P. Stables, N.W. Levin, M.M. Suzman, Am. J. Cardiol. 18 (1966) 370–380.
[3] E.M. Besterman, D.H. Friedlander, Postgrad. Med. J. 41 (1965) 526–535.
[4] C.V.S. Ram, Am. J. Cardiol. 102 (2008) 242–244.
[5] S. Belknap, Evid. Based Med. 13 (2008) 50.
[6] D. Patakas, V. Argiropoulou, G. Louridas, V. Tsara, Thorax 38 (1983) 108–112.
[7] H.S. Bevinakatti, A.A. Banerji, J. Org. Chem. 56 (1991) 5372–5375.
[8] S.V. Darnle, P.N. Patil, M.M. Salunkhe, Synth. Commun. 29 (1999) 3855–3862.
[9] A. Kamal, M. Sandbhor, A. Ali Shaik, Bioorg. Med. Chem. Lett. 14 (2004) 4581–4583.
[10] R.A. Veloo, G.-J. Koomen, Tetrahedron: Asymmetry 4 (1993) 2401–2404.
[11] H. Sasai, N. Itoh, T. Suzuki, M. Shibasaki, Tetrahedron Lett. 34 (1993) 855–858.
[12] Y.-F. Wang, S.-T. Chen, K.K.-C. Liu, C.-H. Wong, Tetrahedron Lett. 30 (1989) 1917–1920.
[13] O. Barbosa, C. Ariza, C. Ortiz, R. Torres, New Biotechnol. 27 (2010) 844–850.
[14] T.-W. Chiou, C.-C. Chang, C.-T. Lai, D.-F. Tai, Bioorg. Med. Chem. Lett. 7 (1997) 433–436.
[15] R. Ávila-González, M. Pérez-Gilabert, F. García-Carmona, J. Biosci. Bioeng. 100 (2005) 423–428.
[16] R. Ávila, R. Ruiz, D. Amaro-González, O. Díaz, J.A. González, A.J. Núñez, Lat. Am. Appl. Res. 35 (2005) 307–311.
[17] A. Ghanem, Tetrahedron 63 (2007) 1721–1754.
[18] A.M. Escorcia, D. Molina, M.C. Daza, M. Doerr, J. Mol. Catal. B: Enzym. 98 (2013) 21–29.
[19] P.-O. Syrén, K. Hult, Chembiochem 11 (2010) 802–810.
[20] G.A. Worth, F. Nardi, R.C. Wade, J. Phys. Chem. B 102 (1998) 6260–6272.
[21] L.S.D. Caves, J.D. Evanseck, M. Karplus, Protein Sci. 7 (1998) 649–666.
[22] P. Trodler, R.D. Schmid, J. Pleiss, BMC Struct. Biol. 9 (2009) 38.
[23] T.C. Bruice, Acc. Chem. Res. 35 (2002) 139–148.
[24] S. Hur, T.C. Bruice, J. Am. Chem. Soc. 125 (2003) 5964–5972.
[25] M.A.J. Veld, L. Fransson, A.R.A. Palmans, E.W. Meijer, K. Hult, Chembiochem 10 (2009) 1330–1334.
[26] M. Svedendahl, P. Carlqvist, C. Branneby, O. Allnér, A. Frise, K. Hult, P. Berglund, T. Brinck, Chembiochem 9 (2008) 2443–2451.
[27] J. Uppenberg, M.T. Hansen, S. Patkar, T.A. Jones, Structure 2 (1994) 293–308.
[28] S. Raza, L. Fransson, K. Hult, Protein Sci. 10 (2001) 329–338.
[29] F. Hæffner, T. Norin, K. Hult, Biophys. J. 74 (1998) 1251–1262.
[30] P. Trodler, J. Pleiss, BMC Struct. Biol. 8 (2008) 9.
[31] B.R. Brooks, C.L. Brooks, A.D. Mackerell, L. Nilsson, R.J. Petrella, B. Roux, Y. Won, G. Archontis, C. Bartels, S. Boresch, A. Caflisch, L. Caves, Q. Cui, A.R. Dinner, M. Feig, S. Fischer, J. Gao, M. Hodoscek, W. Im, K. Kuczera, T. Lazaridis, J. Ma, V. Ovchinnikov, E. Paci, R.W. Pastor, C.B. Post, J.Z. Pu, M. Schaefer, B. Tidor, R.M. Venable, H.L. Woodcock, X. Wu, W. Yang, D.M. York, M. Karplus, J. Comput. Chem. 30 (2009) 1545–1614.
[32] A.D. MacKerell, M. Feig, C.L. Brooks, J. Comput. Chem. 25 (2004) 1400–1415.
[33] A.D. MacKerell, D. Bashford, M. Bellott, R.L. Dunbrack, J.D. Evanseck, M.J. Field, S. Fischer, J. Gao, H. Guo, S. Ha, D. Joseph-McCarthy, L. Kuchnir, K. Kuczera, F.T.K. Lau, C. Mattos, S. Michnick, T. Ngo, D.T. Nguyen, B. Prodhom, W.E. Reiher, B. Roux, M. Schlenkrich, J.C. Smith, R. Stote, J. Straub, M. Watanabe, J. Wiorkiewicz-Kuczera, D. Yin, M. Karplus, J. Phys. Chem. B 102 (1998) 3586–3616.
[34] M. Elstner, D. Porezag, G. Jungnickel, J. Elsner, M. Haugk, T. Frauenheim, S. Suhai, G. Seifert, Phys. Rev. B 58 (1998) 7260–7268.
[35] J.-P. Ryckaert, G. Ciccotti, H.J. Berendsen, J. Comput. Phys. 23 (1977) 327–341.
[36] R.H. Stote, D.J. States, M. Karplus, J. Chim. Phys. 88 (1991) 2419–2433.
[37] C. Oger, Z. Marton, Y. Brinkmann, V. Bultel-Ponceí, T. Durand, M. Graber, J.-M. Galano, J. Org. Chem. 75 (2010) 1892–1897.
[38] E.B. De Oliveira, C. Humeau, L. Chebil, E.R. Maia, F. Dehez, B. Maigret, M. Ghoul, J.-M. Engasser, J. Mol. Catal. B: Enzym. 59 (2009) 96–105.
[39] I. Vallikivi, L. Fransson, K. Hult, I. Järving, T. Pehk, N. Samel, V. Tõugu, L. Villo, O. Parve, J. Mol. Catal. B: Enzym. 35 (2005) 62–69.
[40] C. Bidouil, E.B. De Oliveira, L. Chebil, E.R. Maia, B. Maigret, E. Ronat-Heidt, M. Ghoul, J.-M. Engasser, C. Humeau, J. Biotechnol. 156 (2011) 203–210.
[41] J.H. Park, H.J. Ha, W.K. Lee, T. Généreux-Vincent, R.J. Kazlauskas, Chembiochem 10 (2009) 2213–2222.
[42] W. Humphrey, A. Dalke, K. Schulten, J. Mol. Graph. 14 (1996) 33–38.
[43] M.R. Ganjalikhany, B. Ranjbar, A.H. Taghavi, T. Tohidi Moghadam, PLOS ONE 7 (2012) e40327.
[44] M. Skjøt, L. De Maria, R. Chatterjee, A. Svendsen, S.A. Patkar, P.R. Østergaard, J. Brask, Chembiochem 10 (2009) 520–527.
[45] M. Nishio, Phys. Chem. Chem. Phys. 13 (2011) 13873–13900.
[46] E. García-Urdiales, N. Ríos-Lombardía, J. Mangas-Sánchez, V. Gotor-Fernández, V. Gotor, Chembiochem 10 (2009) 1830–1838.
[47] T. Ema, Y. Nakano, D. Yoshida, S. Kamata, T. Sakai, Org. Biomol. Chem. 10 (2012) 6299–6308.
[48] M. Yamakawa, I. Yamada, R. Noyori, Angew. Chem. Int. Ed. 40 (2001) 2818–2821.
[49] Y. Zhang, J. Kua, J.A. McCammon, J. Phys. Chem. B 107 (2003) 4459–4463.